

## **Supporting Information**

# **Development of Hybrid Pseudohalide Tin Perovskites for Highly Stable Carbon-Electrode Solar Cells**

*Mohammad Rameez,<sup>1, 2 & 3</sup> Eric Yan-Ru Lin,<sup>1</sup> Putikam Raghunath,<sup>1</sup> Sudhakar Narra,<sup>1</sup>  
Donghoon Song,<sup>1</sup> Ming Chang Lin,<sup>1, 4</sup> Chen Hsiung Hung,<sup>\*,2</sup> and Eric Wei-Guang Diau<sup>\*,1,4</sup>*

<sup>1</sup>Department of Applied Chemistry and Institute of Molecular Science, National Chiao Tung University, 1001 Ta-Hsueh Rd., Hsinchu 30010, Taiwan

<sup>2</sup>Institute of Chemistry, Academia Sinica, Nankang, Taipei 11529, Taiwan.

<sup>3</sup>Sustainable Chemical Science and Technology (SCST), Taiwan International Graduate Program (TIGP), Academia Sinica, Nankang, Taipei 11529, Taiwan.

<sup>4</sup>Center for Emergent Functional Matter Science, National Chiao Tung University, 1001 Ta-Hsueh Rd., Hsinchu 30010, Taiwan

## **AUTHOR INFORMATION**

### **Corresponding Authors**

\* Dr. Eric Wei-Guang Diau

Department of Applied Chemistry and Institute of Molecular Science, National Chiao Tung University, Hsinchu 30010, Taiwan. E-mail: [diau@mail.nctu.edu.tw](mailto:diau@mail.nctu.edu.tw)

\* Dr. Chen-Hsiung Hung

Institute of Chemistry, Academia Sinica, Nankang, Taipei 11529, Taiwan. E-mail:  
[chhung@gate.sinica.edu.tw](mailto:chhung@gate.sinica.edu.tw)

## Methods

### Materials

$\text{Sn}(\text{SCN})_2$  was synthesized with the procedure reported by Filby et.al.<sup>S1</sup> Namely,  $\text{NaSCN}$  (12 g) was dissolved in degassed distilled water and poured into an aqueous solution of  $\text{Sn}(\text{SO}_4)_2$ . The resulting solution was left for crystallization for two days. The obtained white crystals were washed with deionized water and dried overnight in a vacuum oven at 40° C. These dried crystals were used for device fabrication without purification.

Formamidinium iodide (FAI), ethylenediammonium diiodide, phenethylammonium iodide and formamidinium thiocyanate (FASCN) were purchased (Dysol).  $\text{SnF}_2$  (99 %, Sigma-Aldrich),  $\text{SnI}_2$  (99.999 %, Alfa Aesar) were used directly without purification. N,N-dimethylformamide (anhydrous, 99.8% , Sigma-Aldrich) was used as solvent. Methyl phenyl ether (anhydrous, 99.8%, Sigma-Aldrich) and benzotrifluoride (anhydrous, 99.8% , Sigma-Aldrich) were used for solvent extraction (SE).

### Computational methods

We investigated computationally the effect of incorporation of SCN into the iodide sites of the orthorhombic perovskite  $\text{FASnI}_3$  using the Vienna ab initio simulation package (VASP). To predict the total energy, the exchange-correlation function treated with the generalized-gradient approximation (GGA) and the Perdew-Burke-Ernzerhof formulation (PBE) was applied throughout the system.<sup>S2</sup> The valence-electron configurations considered in this calculation were Sn ( $4\text{d}^{10}\text{s}^2\text{p}^2$ ), I ( $5\text{s}^2\text{p}^5$ ), S ( $3\text{s}^2\text{p}^4$ ), C ( $2\text{s}^2\text{p}^2$ ), N ( $2\text{s}^2\text{p}^3$ ) and H ( $1\text{s}$ ). To account for the *van der Waals* interactions between the organic (FA) and other elements of perovskite, we utilized the standard PBE functional augmented with Grimme's semi-empirical dispersion-potential-corrected DFT-D2 method.<sup>S3</sup> The convergence criterion for the self-consistent iteration was  $10^{-5}$  eV. The calculations were carried out with cutoff energy 500 eV

for the plane-wave basis set. Brillouin zone integrals were computed over regular Monkhorst-Pack grids with  $4 \times 4 \times 4$   $k$ -points for all present perovskite models generated for the structural optimization and calculation of the electronic properties. The radius of SCN<sup>-</sup> was taken from Jenkins *et al.*<sup>84</sup> For PDOS calculations, the SCN<sup>-</sup> perovskites were modelled on the crystal structure of FASnI<sub>3</sub> reported by Kanatzidis and co-workers.<sup>85</sup> All positions and lattice parameters were fully relaxed and optimized to a force convergence 0.02 eV Å<sup>-1</sup>. We also performed gas-phase calculations optimized with density-functional theory (wB97XD method) using program Gaussian 09. The basis set used in these calculations was Lanl2dz, which included the D95 double- $\zeta$  basis set for Sn and I along with an effective core potential (ECP, Hay and Wadt) and the 6-311++G(d,p) basis set for main-group elements.

### Characterization of materials and devices

XRD of a thin film coated on ITO substrates was measured with an X-ray diffractometer (XRD, Bruker D8-Advance, Cu K $\alpha$  radiation). Infrared spectra (4000–500 cm<sup>-1</sup>) were recorded on a VERTEX 70 spectrometer with an ATR accessory (Golden Gate diamond) on solid powder samples. UV-visible absorption spectra were recorded (Jasco V-780 UV-vis/NIR spectrophotometer) on a fused-silica substrate. Photoluminescence (PL) experiments were performed (JASCO monochromator, CT-50TFP, f-number 4.3, grating 600 lines mm<sup>-1</sup> blazed at 1000 nm) suitable for NIR measurements. X-ray photoelectron spectra (XPS) were recorded (Thermo K-ALPHA Surface Analysis) of perovskite films coated on ITO substrates. Ultraviolet photoelectron spectra (UPS) were recorded (Thermo Fisher Scientific, ESCALAB Xi<sup>+</sup>); the samples were etched with a beam of ions (1 keV Ar<sup>+</sup>). The samples were biased at -5.0 V to avoid the overlap of low-energy secondary cut-off signals of the instrument and directly transferred from a glove box to avoid sample degradation. All UPS experiments were calibrated with the Fermi edge of a clean gold surface and performed under pressure 10<sup>-9</sup> Torr. To obtain the lifetime of perovskite films we used a time-correlated single-photon-counting

(TCSPC) system (Fluotime 200, PicoQuant) with excitation at 635 nm from a picosecond pulsed-diode laser (LDH-635, PicoQuant, FWHM  $\sim$ 70 ps). The PL temporal profiles were collected at  $850\pm32$  nm, which covers the emission maximum but is at the edge of the sensitive region of the used MCP-PMT (R3809U-50), for all perovskite samples under investigation. To investigate the morphology of the samples we used a field-emission scanning electron microscope (FESEM, Hitachi SU8010).

To characterize the photovoltaic performance of the devices we employed a digital source meter (Keithley 2400) under one-sun illumination (AM 1.5G, 100 mW cm $^{-2}$ ) from a solar simulator (XES-40S1, SAN-E1); the solar spectrum was calibrated with a silicon diode and a KG-5 filter to decrease the mismatch of the spectrum. All measurements were performed with reverse voltage scans ( $V_{OC}$  to 0.0 V) under ambient conditions. The ratios of incident photons to current (IPCE) were recorded with a system comprising a Xe lamp (A-1010, PTi, 150 W) and a monochromator (PTi). The electrochemical impedance spectra (EIS) of all devices were measured with an electrochemical workstation (IM 6, Zahner, Germany) over frequency range 100 mHz - 4 MHz with ac amplitude 10 mV under darkness. The obtained EIS data were fitted (Z-view software) based on an equivalent-circuit model. Contact angles were measured (KRÜSS Easy Drop optical system, KRÜSS GmbH–Germany).

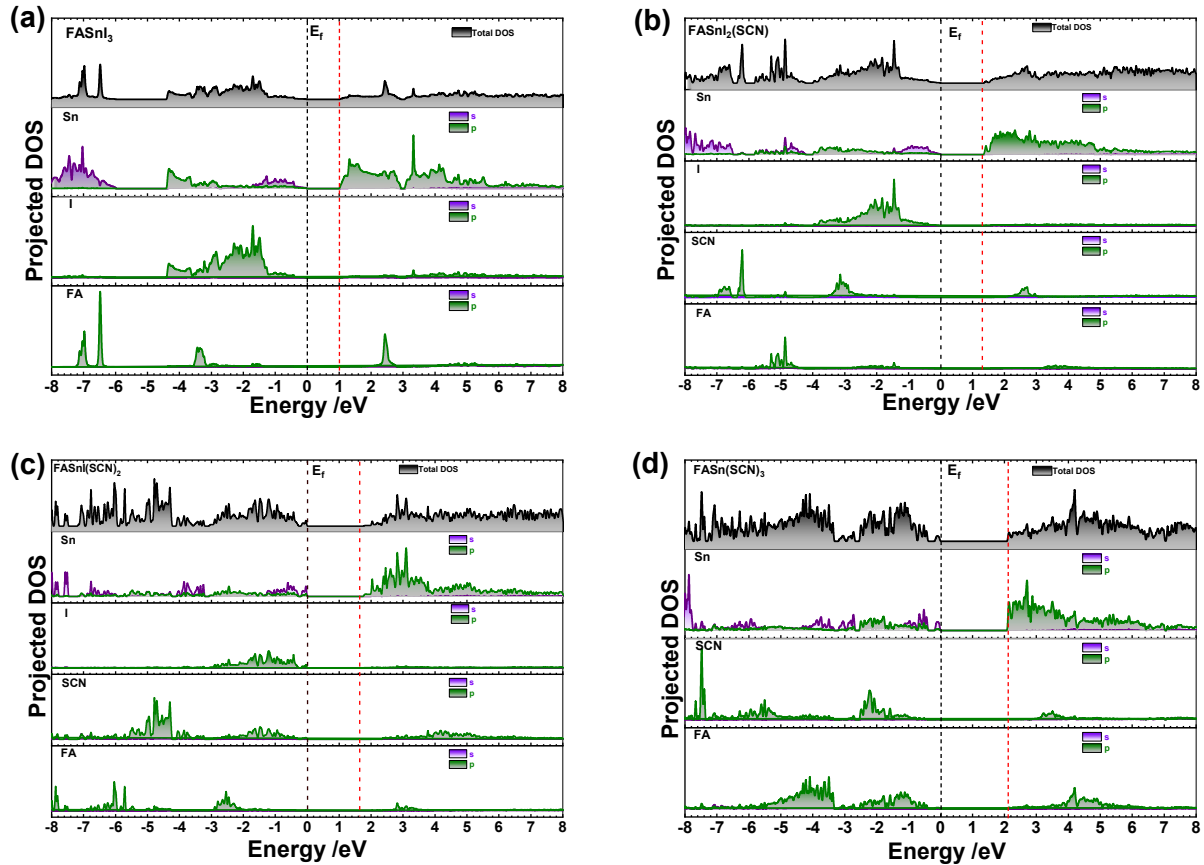


**Figure S1.** Simulated projected density of states (PDOS) of perovskites  $\text{FASnI}_{3-x}(\text{SCN})_x$  with  $x = \text{(a) } 0, \text{(b) } 1, \text{(c) } 2, \text{ and (d) } 3$ . Black dashed lines indicate Fermi energy levels; red dashed lines indicate the conduction-band levels for each system.

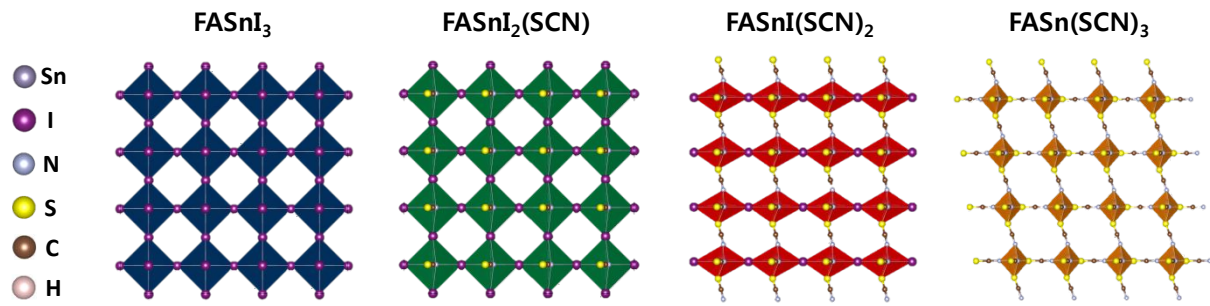


**Figure S2.** DFT simulated crystal structure of  $\text{FASnI}_{3-x}(\text{SCN})_x$  depicting the components of crystal octahedra in the plane

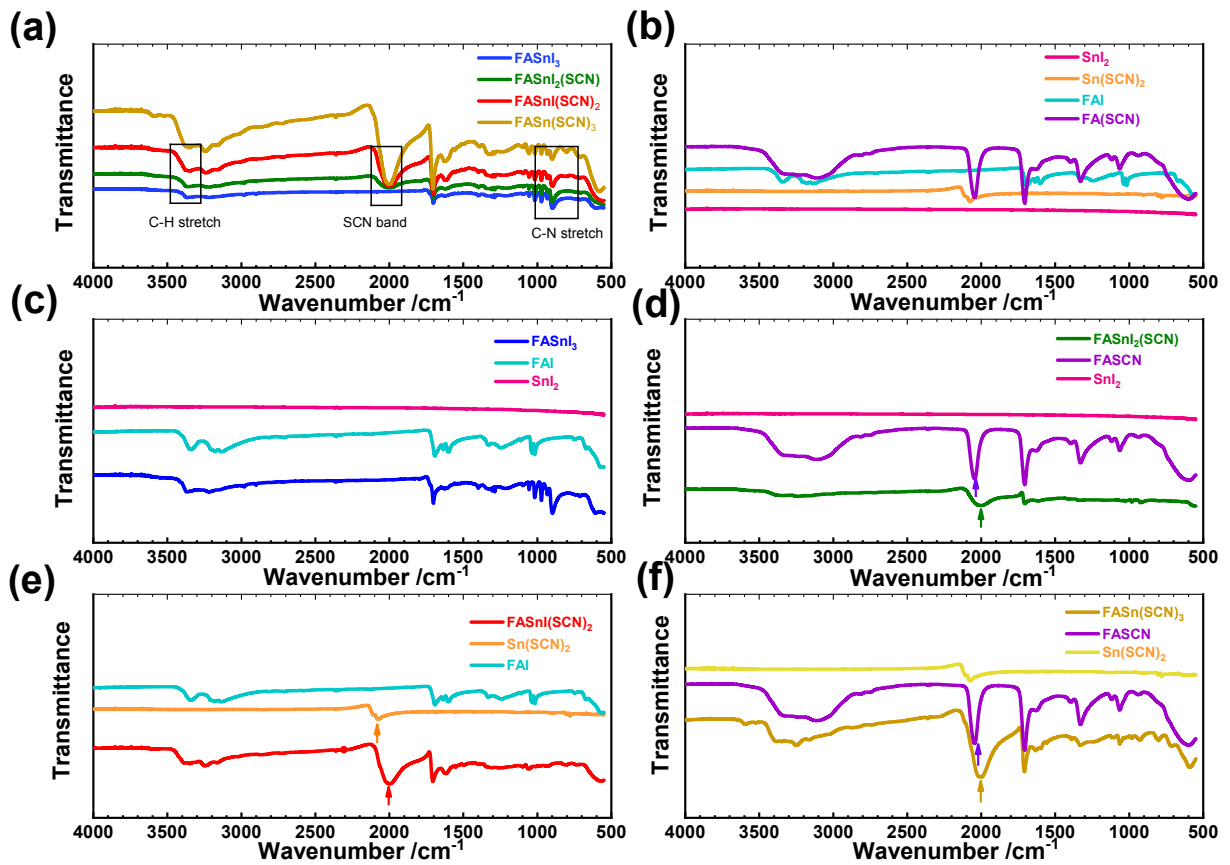


**Figure S3.** (a-f) FTIR spectra of FASnI<sub>3-x</sub>(SCN)<sub>x</sub> perovskites and their corresponding precursors

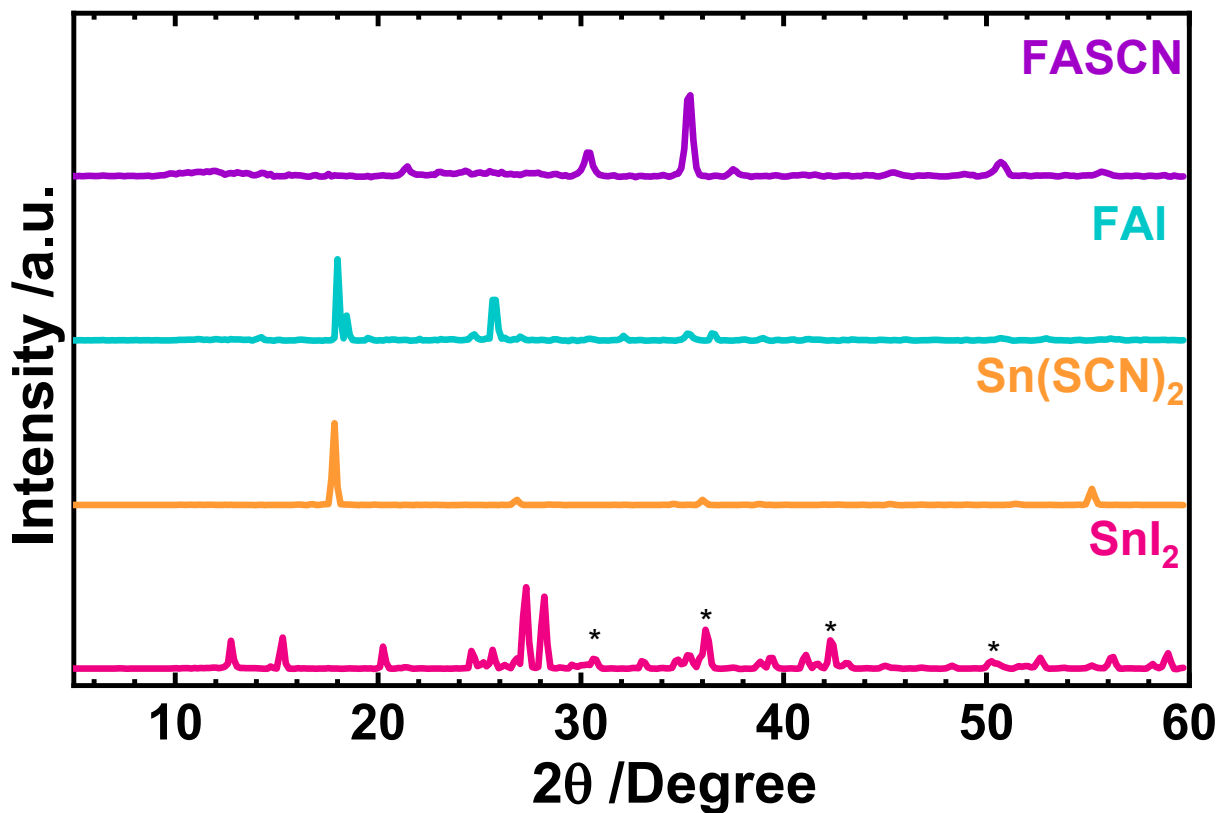


**Figure S4.** Thin-film XRD patterns of all perovskite precursors used to make perovskite thin films. The asterisks label the diffraction signals of ITO substrate.

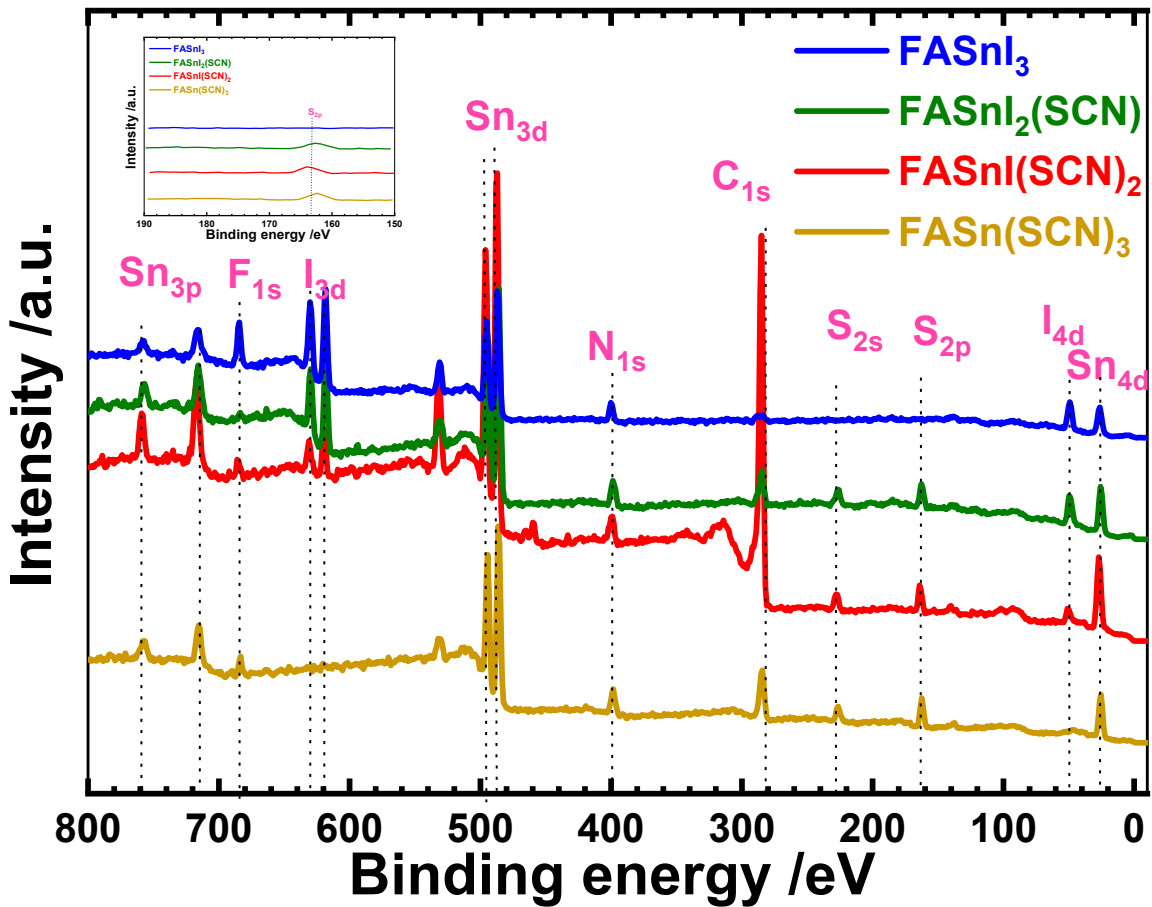


**Figure S5.** Plots of the XPS survey scan of  $\text{FASnI}_{3-x}(\text{SCN})_x$  ( $x = 0-3$ ) perovskite thin films deposited on Si substrates. Inset shows the absence of S in a pristine  $\text{FASnI}_3$  film.

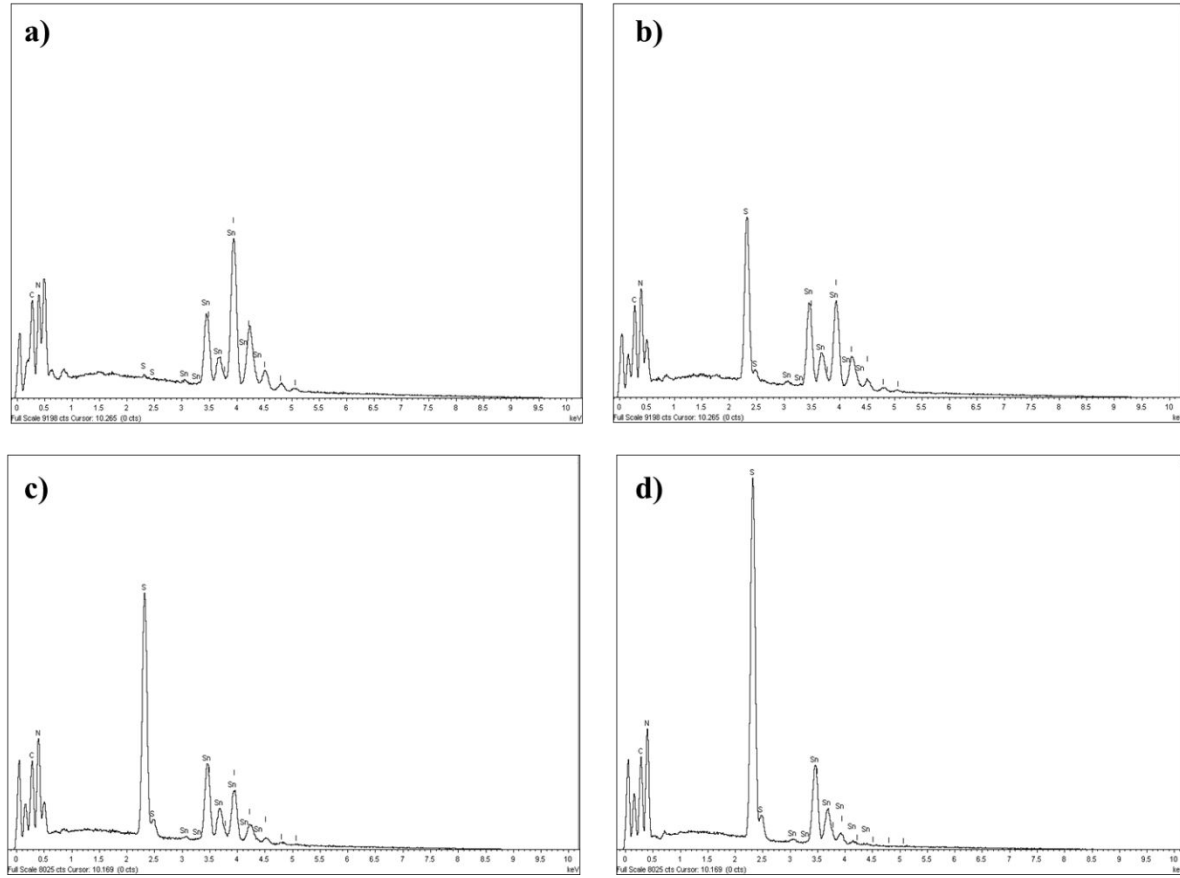


**Figure S6.** a-d) The EDX spectra for the FASnI<sub>3-x</sub>(SCN)<sub>x</sub> ( $x = 0-3$ ) perovskites.

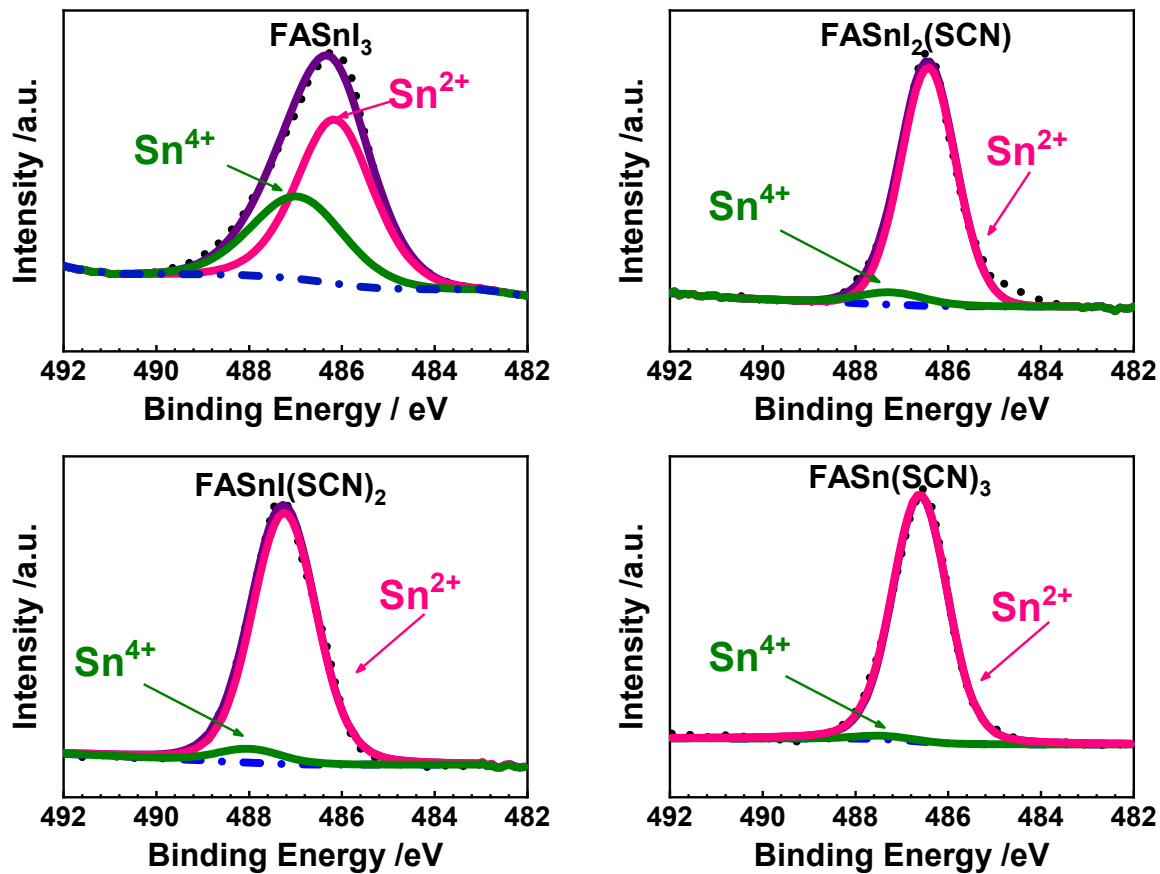


**Figure S7.** XPS of Sn 3d recorded for bulk  $\text{FASnI}_{3-x}(\text{SCN})_x$  ( $x = 0\text{--}3$ ) samples after plasma etching. The two lines deconvoluted from the measured spectra comprise  $\text{Sn}^{4+}$  line (green) at slightly greater binding energy with each main  $\text{Sn}^{2+}$  line (magenta).

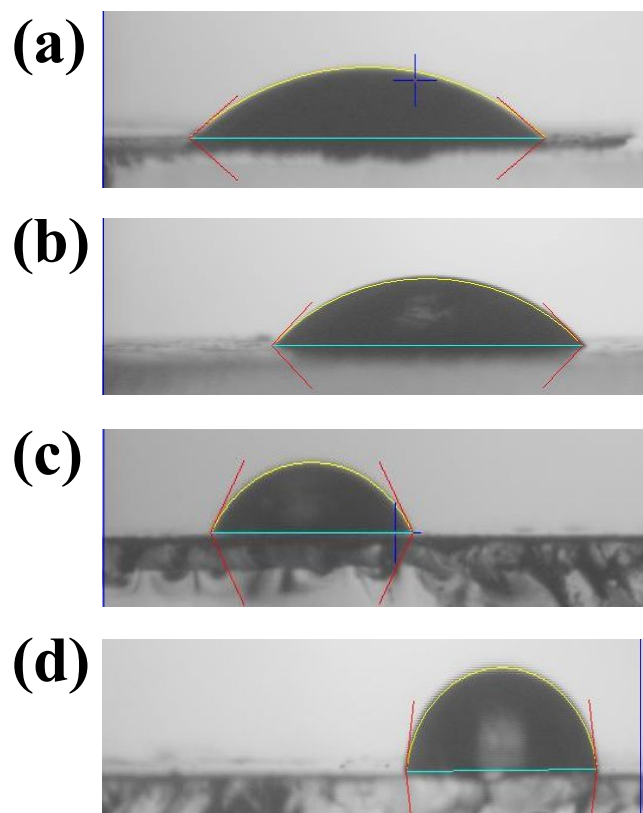


**Figure S8.** Water contact angle of perovskite films: (a) FASnI<sub>3</sub> 36.2°, (b) FASnI<sub>2</sub>(SCN) 46.8°, (c) FASnI(SCN)<sub>2</sub> 60.8°, (d) FASn(SCN)<sub>3</sub> 81.9°.

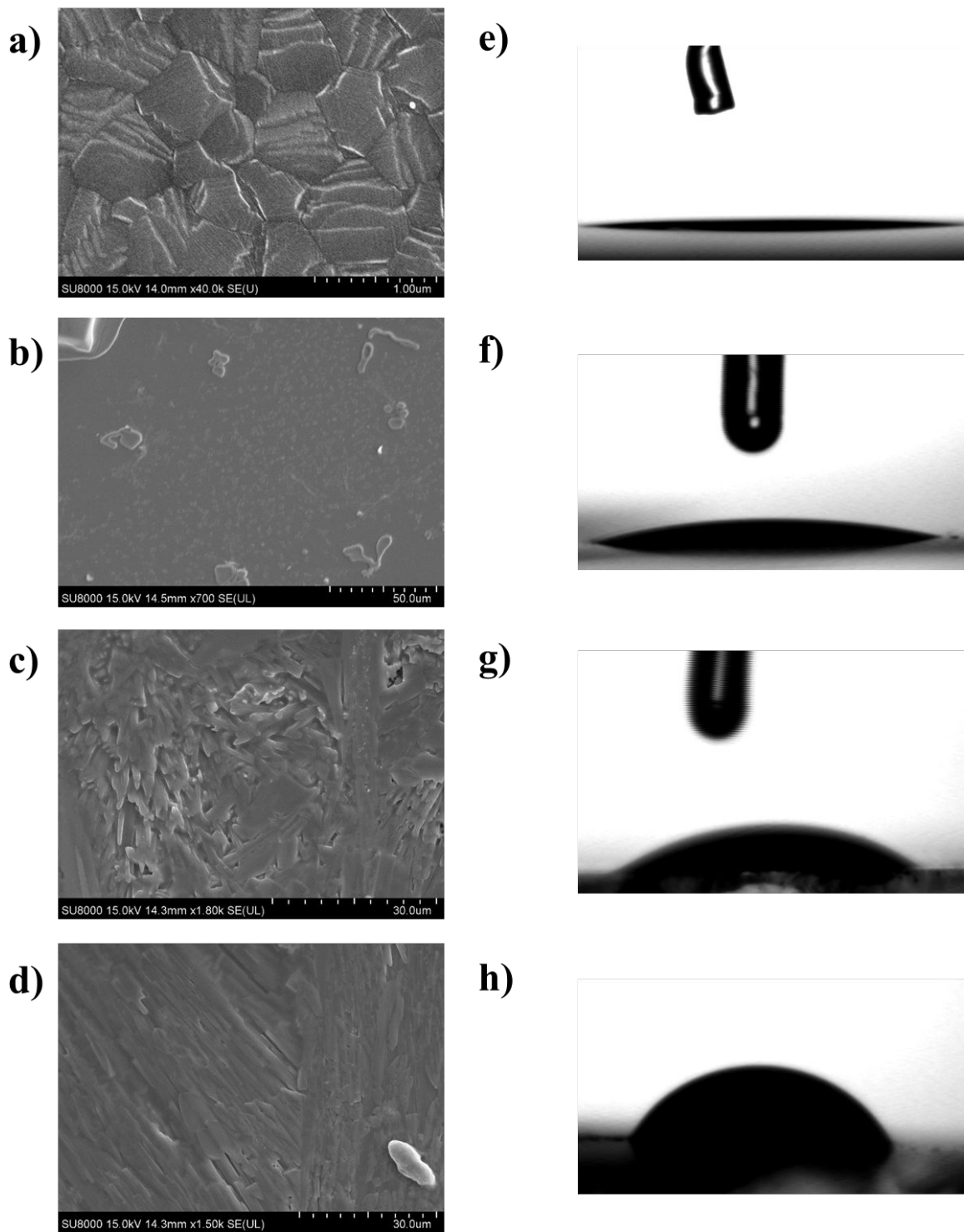


**Figure S9.** a-d) Top-view SEM images of the FASnI<sub>3-x</sub>(SCN)<sub>x</sub> thin films prepared with  $x = 0$  -3 based on initial stoichiometric ratios; e-h) contact angles of precursor solutions: e) 6° for FAI+SnI<sub>2</sub>; f) 14.38° for FASCN+SnI<sub>2</sub>; g) 26.51° for FAI+Sn(SCN)<sub>2</sub>; h) 41.70° for FASCN+Sn(SCN)<sub>2</sub>.

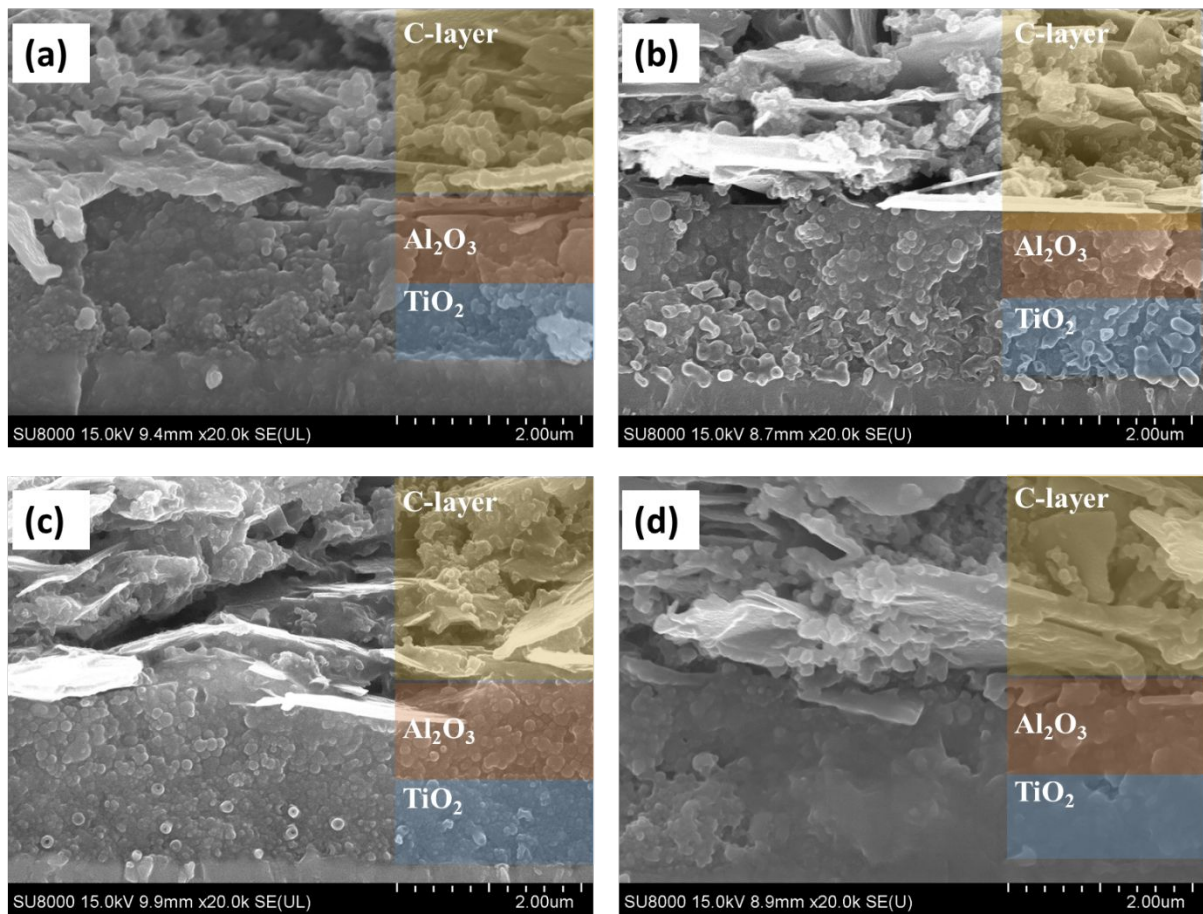


**Figure S10.** SEM cross-section images of mesoporous-carbon electrode devices (a) FASnI<sub>3</sub>, (b) FASnI<sub>2</sub>(SCN), (c) FASnI(SCN)<sub>2</sub>, and (d) FASn(SCN)<sub>3</sub>.

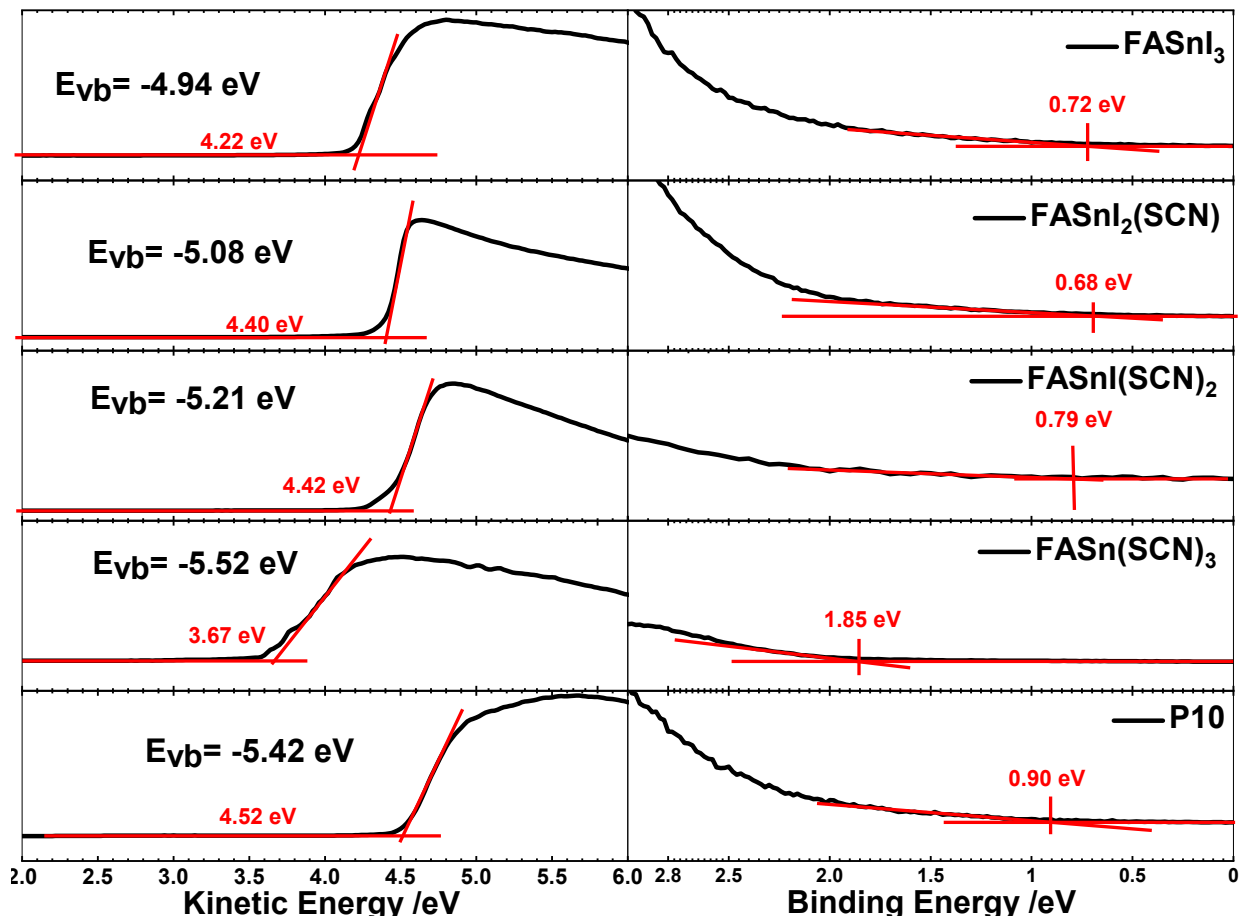


**Figure S11.** UPS of  $\text{FASnI}_{3-x}(\text{SCN})_x$ . The left plots illustrate the work function of each species determined from the spectral onsets. The right plots show the energy gap from the work function to the valence band (VB) of each species on spectral onsets with the zero point representing the work function.

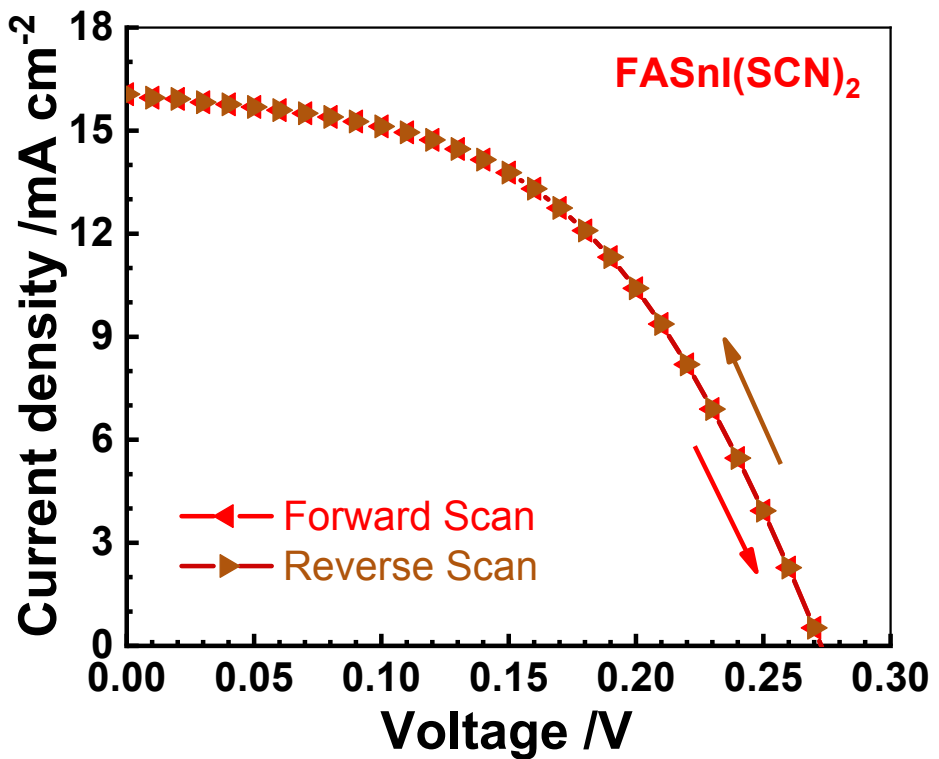


**Figure S12.**  $J-V$  characteristics of a  $\text{FASnI}(\text{SCN})_2$  device with two scan directions: forward scan (from short circuit to open circuit) and reverse scan (from open circuit to short circuit).

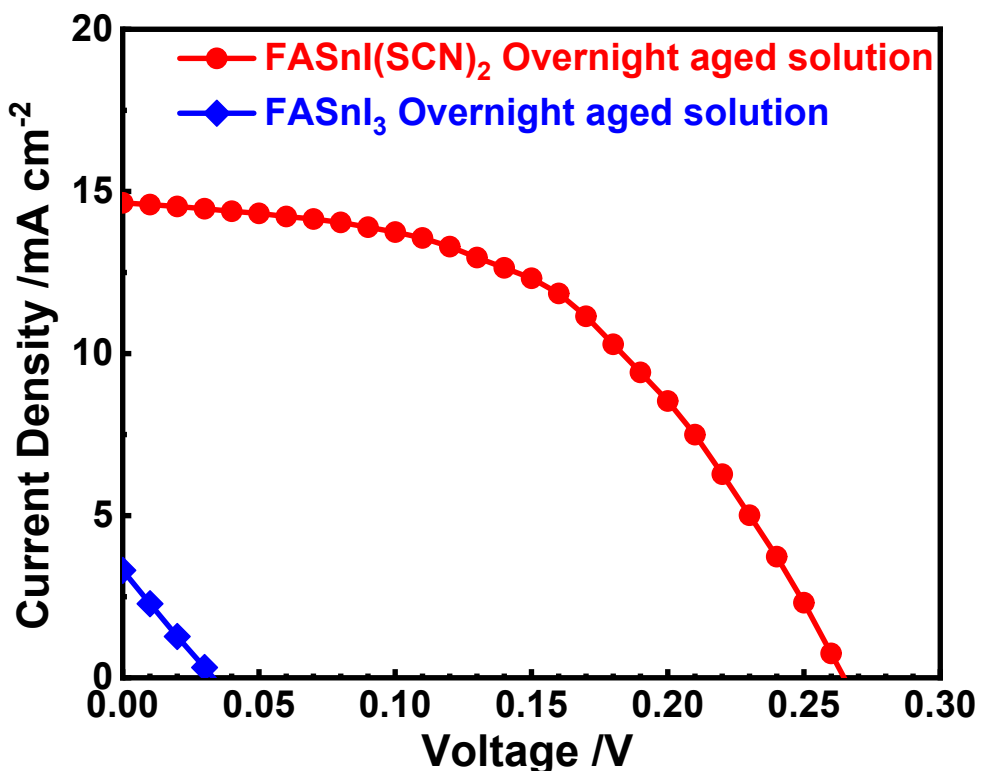


**Figure S13.** (a) Photovoltaic performance of FASnI<sub>3</sub> and FASnI(SCN)<sub>2</sub> devices fabricated with solutions aged overnight.

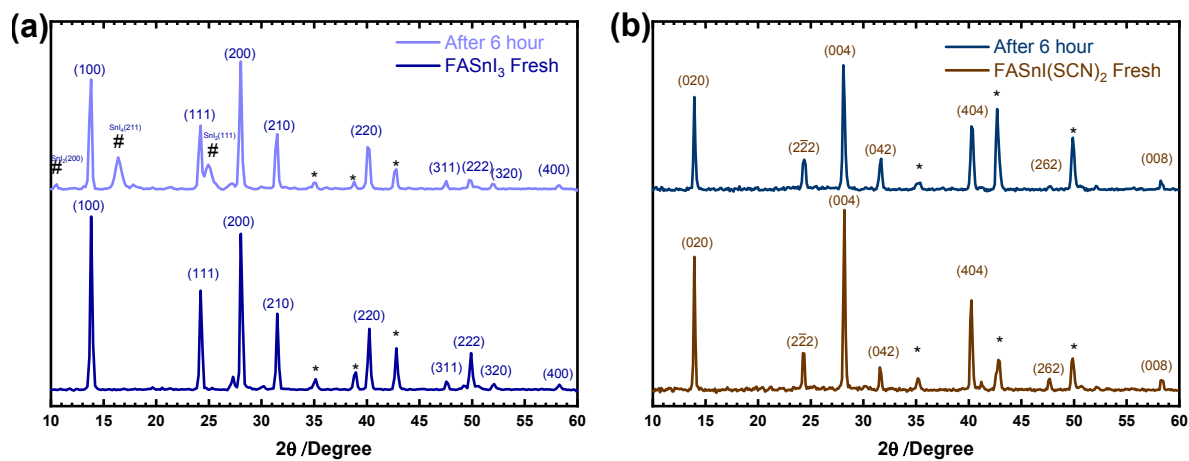


**Figure S14.** XRD test of stability of (a) FASnI<sub>3</sub> and (b) FASnI(SCN)<sub>2</sub> films for fresh and after storage for 6 h under ambient conditions. “\*” labels diffraction signals of ITO; “#” indicates new signals of iodide salts of Sn.

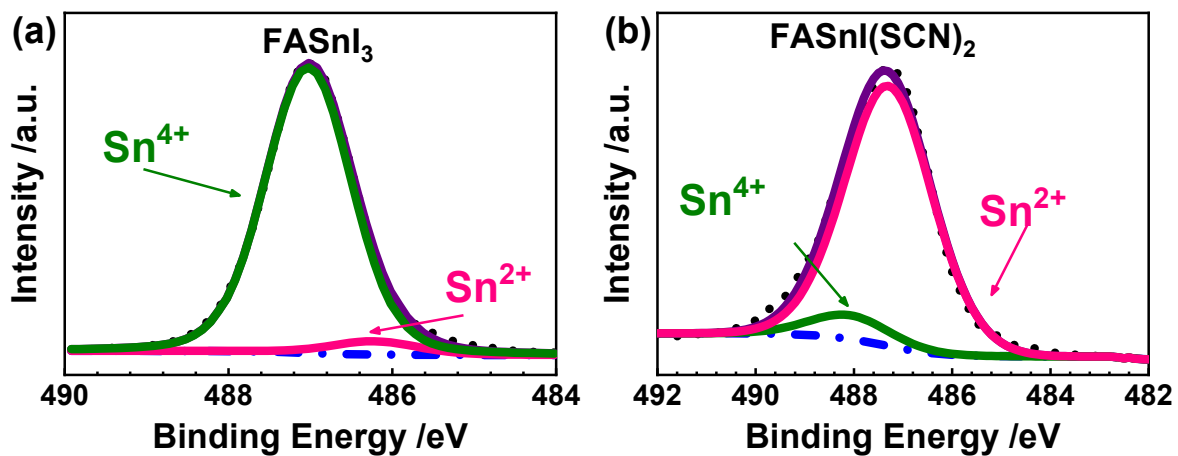


**Figure S15.** XPS test of stability of a) FASnI<sub>3</sub> and b) FASnI(SCN)<sub>2</sub> after storage overnight (15 h) under ambient conditions. For FASnI(SCN)<sub>2</sub>, Sn<sup>2+</sup> at the surface was 7.6 %; for FASnI<sub>3</sub>, Sn<sup>2+</sup> at surface was 95.6 %.

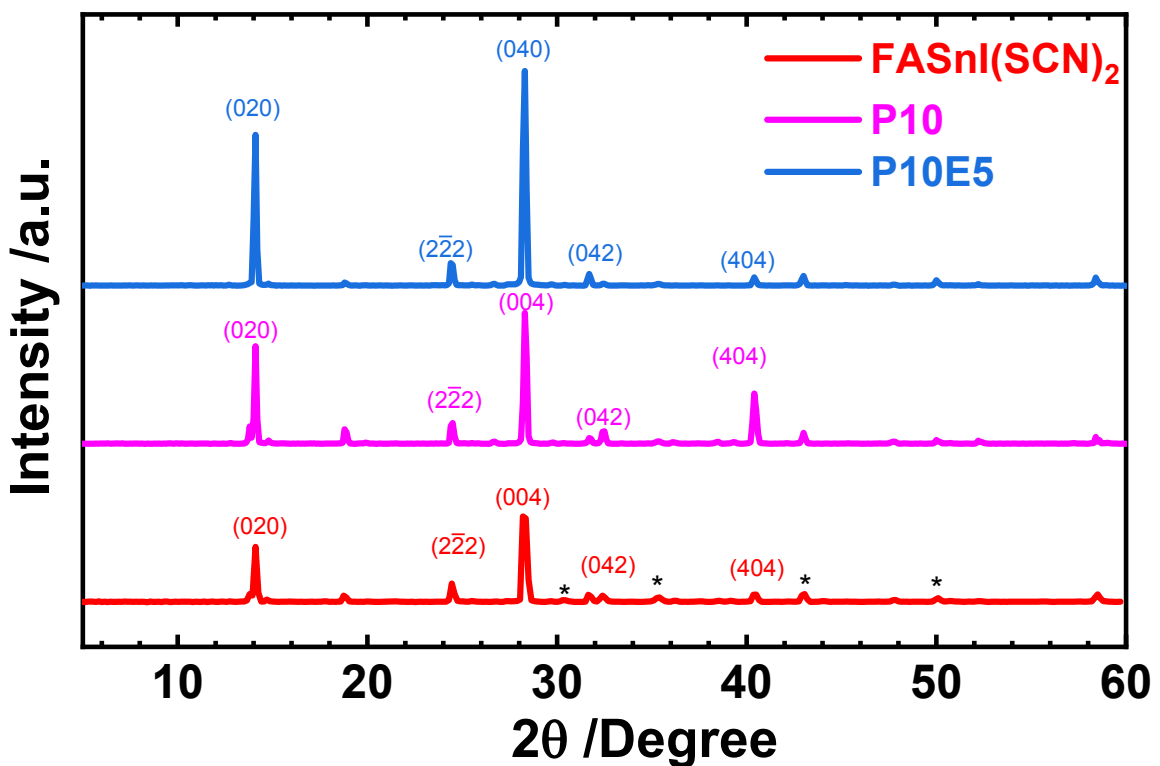


**Figure S16.** Experimental thin-film XRD patterns of FASnI(SCN)<sub>2</sub>, P10 and P10E5 thin films on ITO substrates. The asterisks label the diffraction signals of ITO.

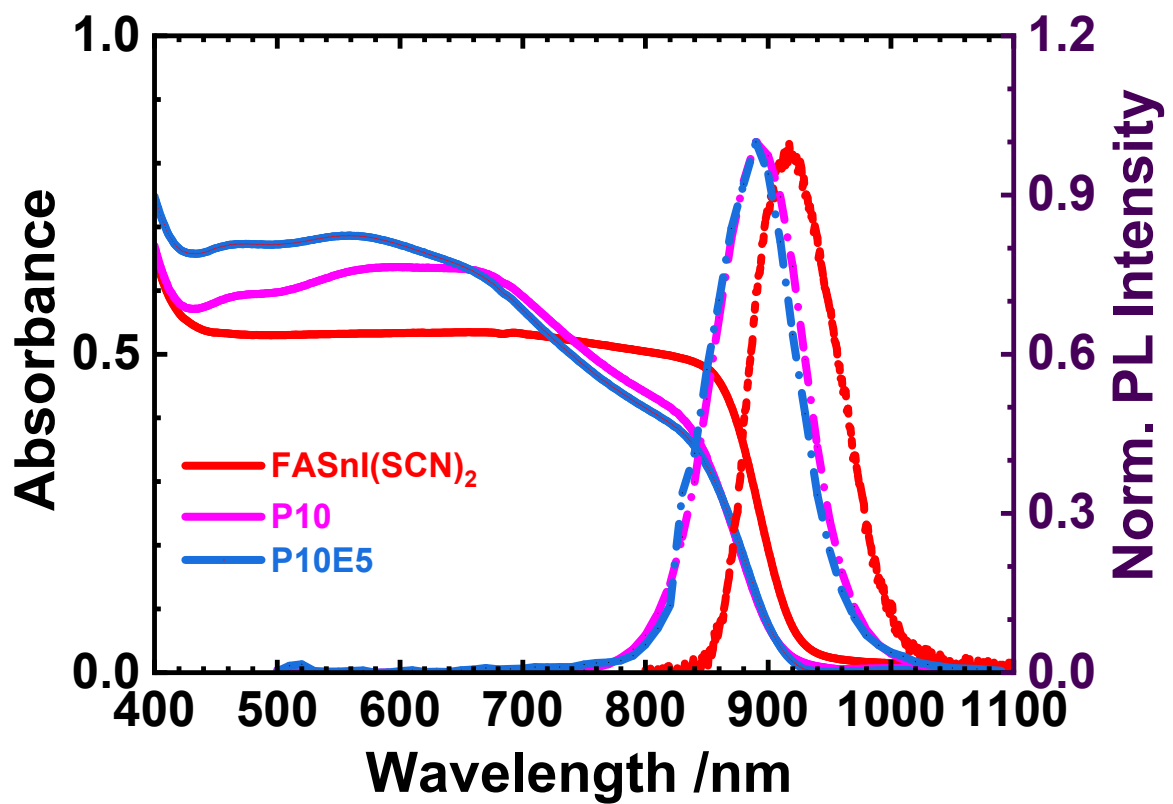


**Figure S17.** Absorption (solid curves) and normalized PL (dashed curves) spectra of FASnI(SCN)<sub>2</sub>, P10 and P10E5 films deposited on glass substrates.

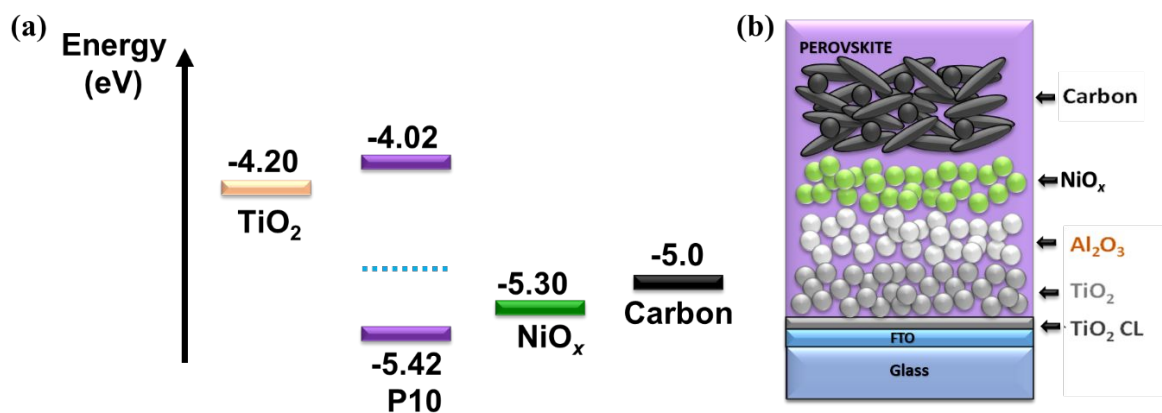


**Figure S18.** (a) Energy diagrams (energy/eV with respect to vacuum) of P10 film and other layers. The positions of the WF are indicated as dashed lines. (b) Schematic representation of the mesoscopic TiO<sub>2</sub>/Al<sub>2</sub>O<sub>3</sub>/NiO<sub>x</sub>/carbon-based device.

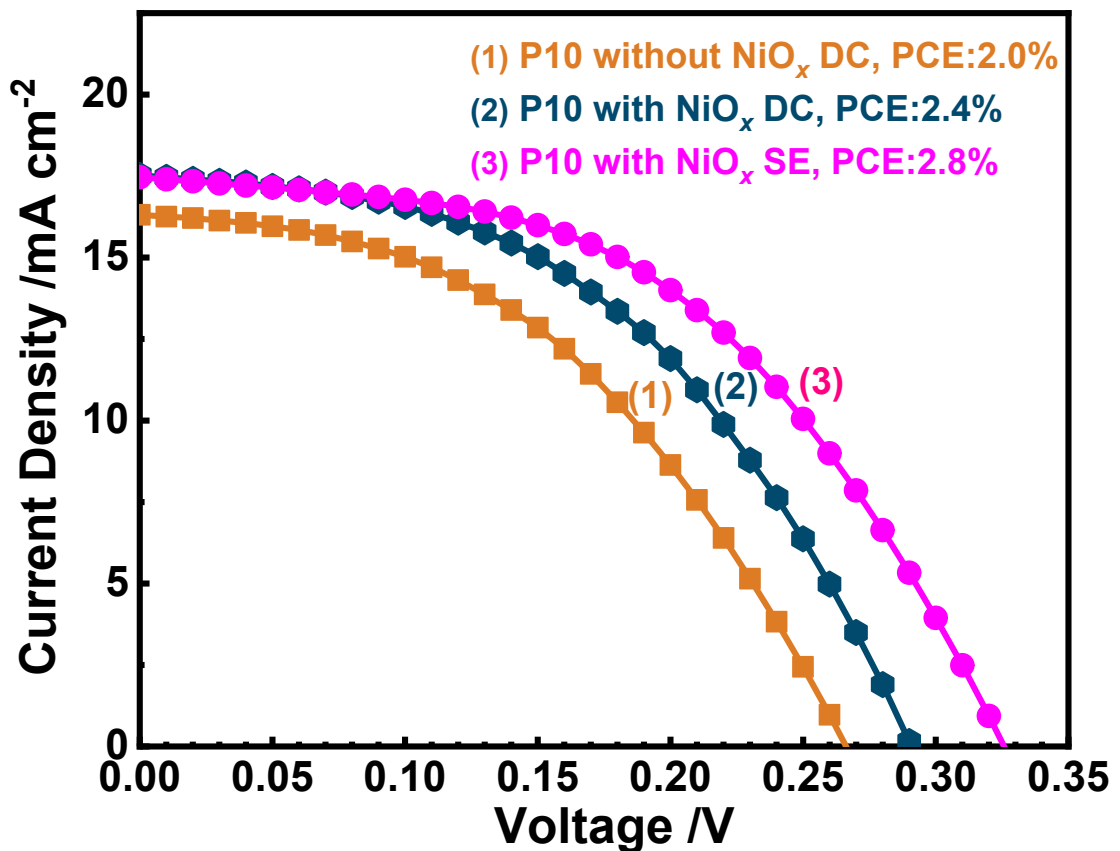


**Figure S19.** Photovoltaic performance of P10 devices fabricated with the drop-casting (DC) and solvent-extraction (SE) method.

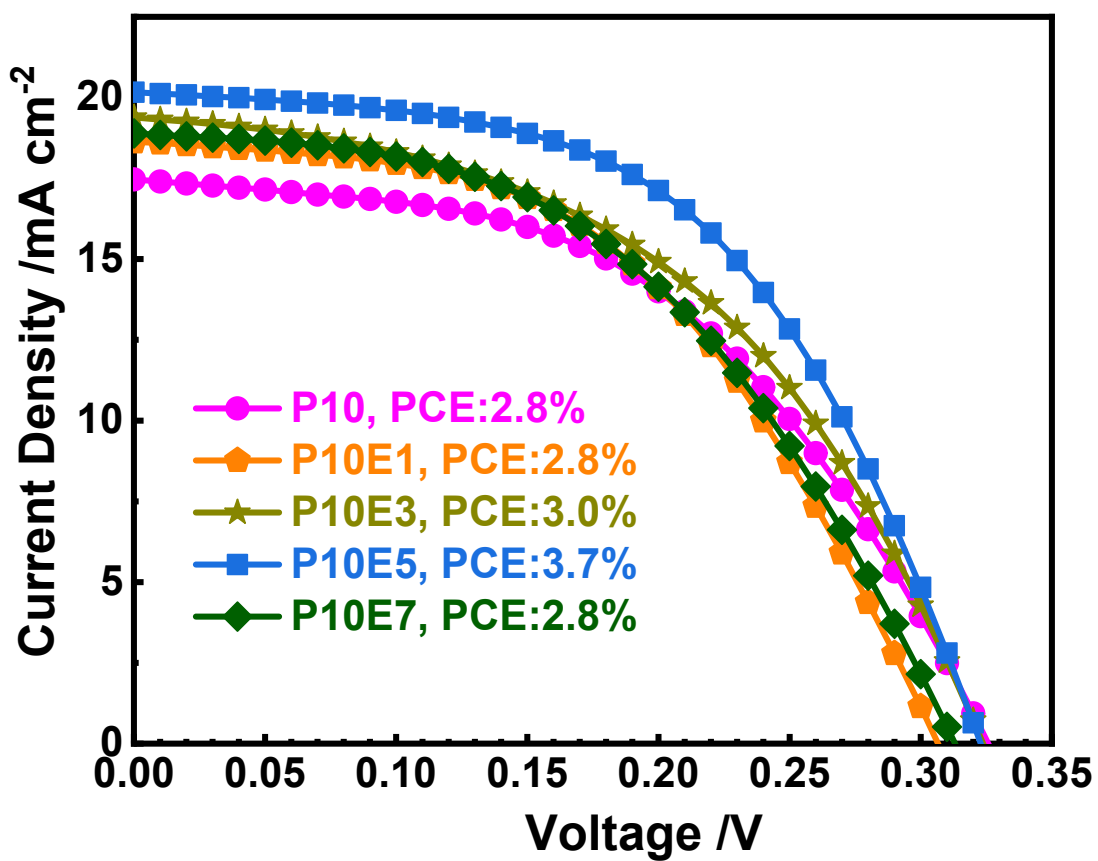


**Figure S20.** Photovoltaic performance of P10 devices fabricated with varied percentage of EDAI<sub>2</sub>.

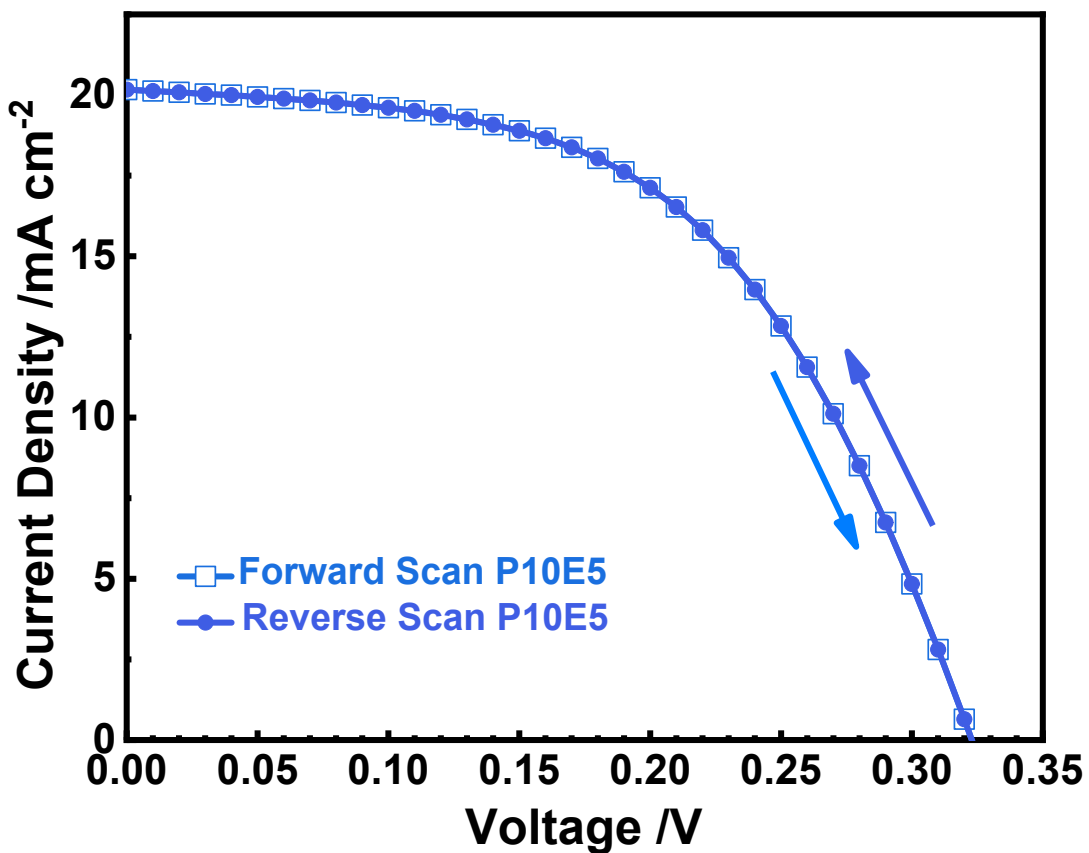


**Figure S21.**  $J-V$  characteristics of a P10E5 device with two scan directions: forward scan (from short circuit to open circuit) and reverse scan (from open circuit to short circuit).

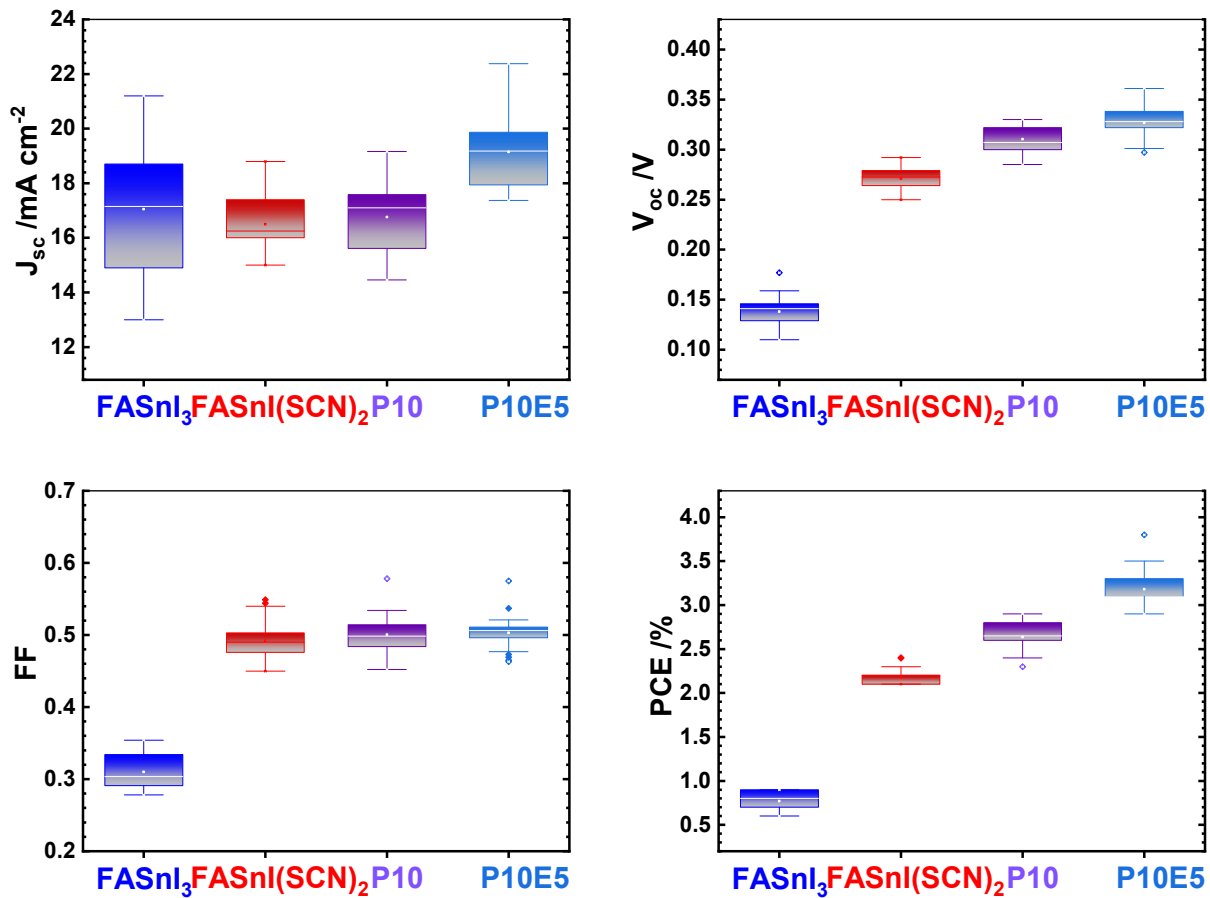


**Figure S22.** Box-plot statistical distribution for 30 devices each for FASnI<sub>3</sub>, FASnI(SCN)<sub>2</sub>, P10 and P10E5 perovskite solar cells.

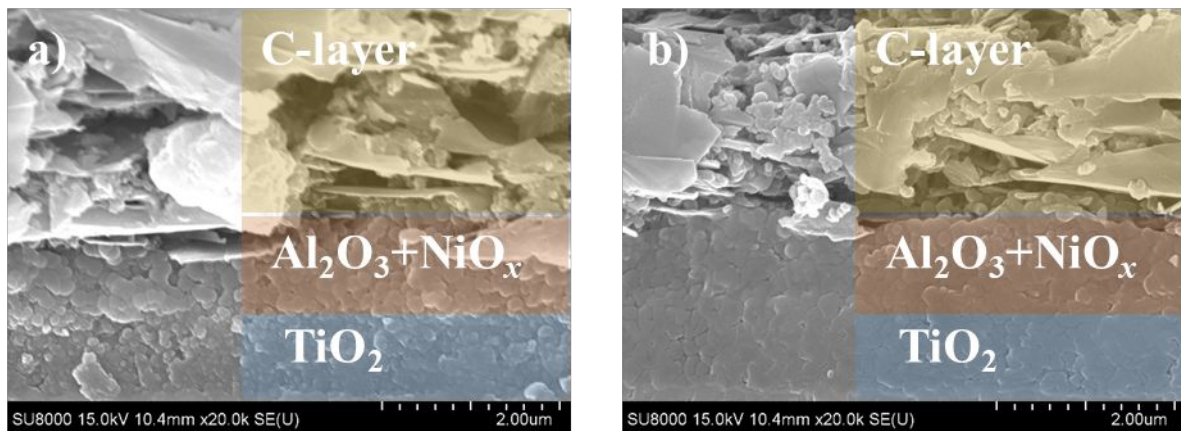


**Figure S23.** SEM cross-sectional images of mesoporous-carbon electrode devices of (a) P10 and (b) P10E5 devices fabricated using the solvent-extraction (SE) method.

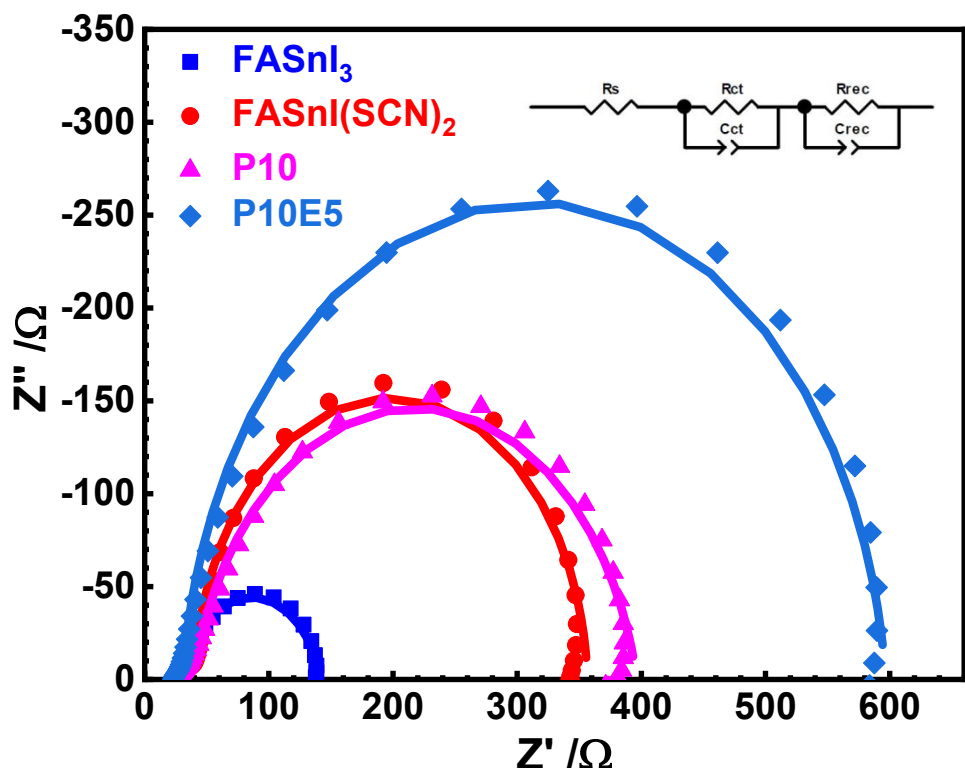


**Figure S24.** Nyquist plots of FASnI<sub>3</sub>, FASnI(SCN)<sub>2</sub>, P10 and P10E5 perovskite solar cells in darkness recorded at the open-circuit voltage.

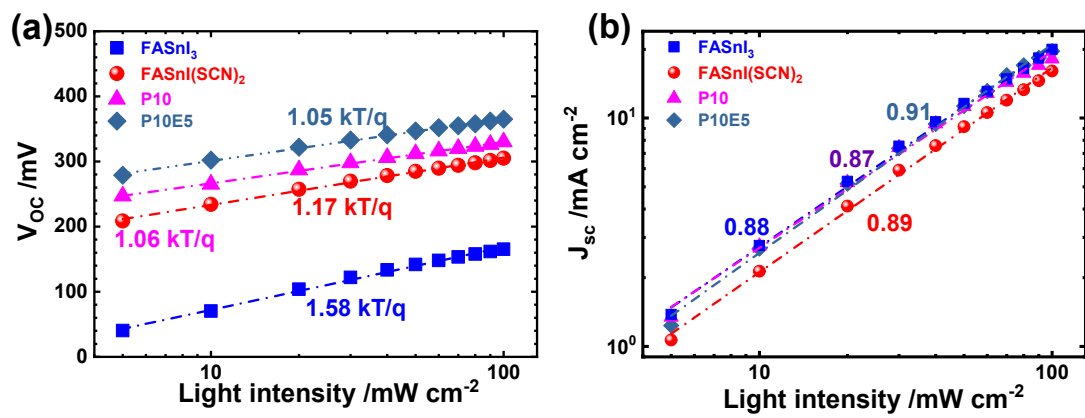


**Figure S25.** Dependence on light intensity of (a) open-circuit voltage ( $V_{oc}$ ) and (b) short-circuit current density ( $J_{sc}$ ) for FASnI<sub>3</sub>, FASnI(SCN)<sub>2</sub>, P10 and P10E5 devices.

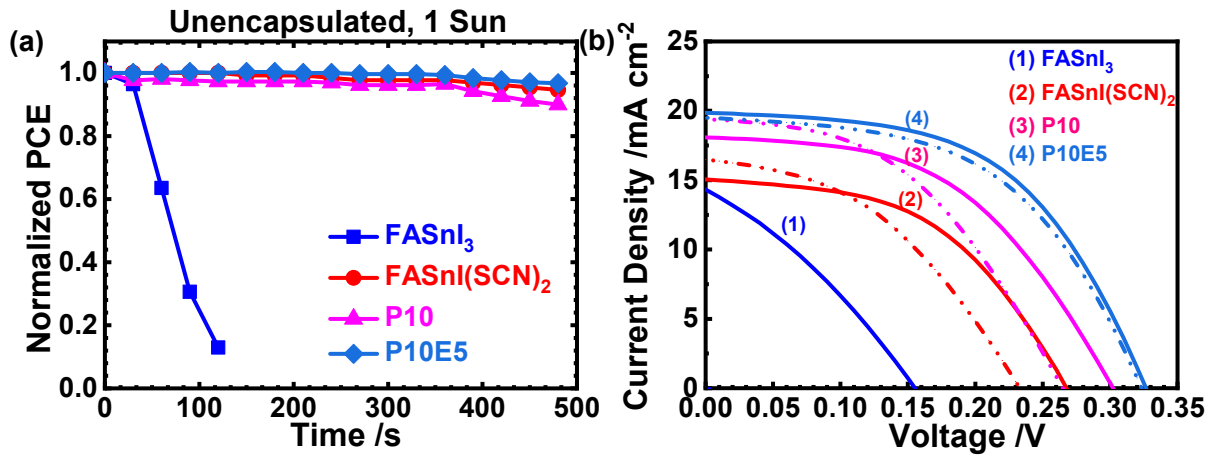


**Figure S26.** (a) Photovoltaic performance stability of unencapsulated FASnI<sub>3</sub>, FASnI(SCN)<sub>2</sub>, P10 and P10E5 devices under sustained illumination (AM1.5G) soaking without encapsulation under ambient conditions with RH~65 %. (b) Stability of corresponding perovskite solar cells without encapsulation in an ambient environment with 65 % relative humidity at 25°C stored in darkness. Solid  $J$ - $V$  curves were obtained from the fresh devices; the dashed  $J$ - $V$  curves obtained from the devices aged 6 h.

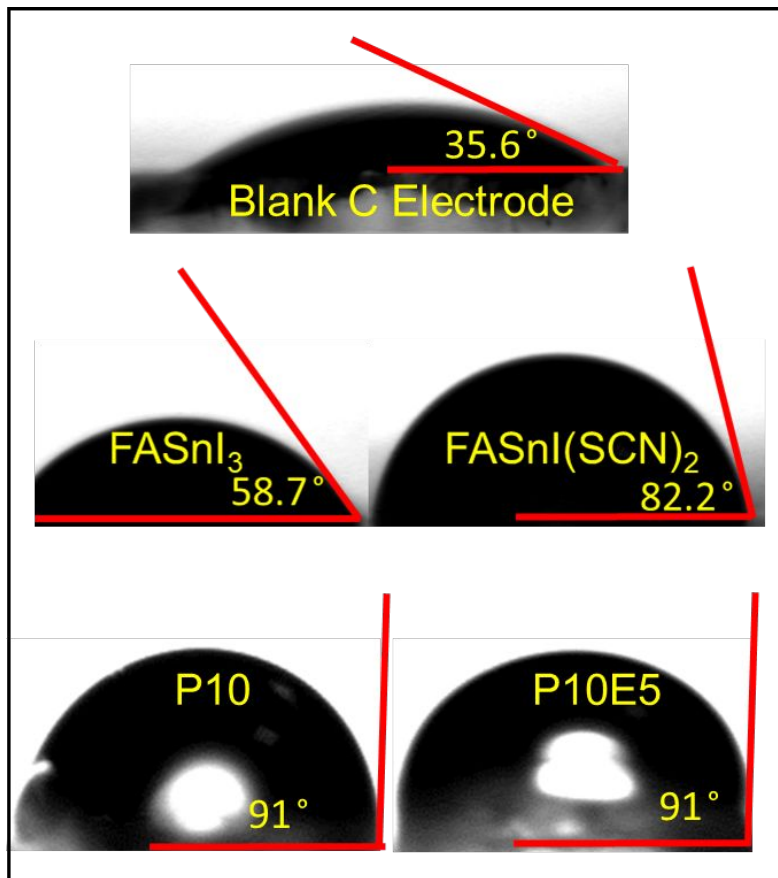


**Figure S27.** Water contact angles on blank C-electrode, FASnI<sub>3</sub>, FASnI(SCN)<sub>2</sub>, P10 and P10E5 devices.

**Table S1.** Lattice parameters of  $\text{FASnI}_{3-x}(\text{SCN})_x$  conventional cells, calculated with the PBE function, with lattice length/ $\text{\AA}$  and angle/deg.

$x$	Materials	$a$	$b$	$c$	$\alpha$	$\beta$	$\gamma$	Crystal System
0	$\text{FASnI}_3$	12.642	12.642	12.642	90.00	90.00	90.00	Cubic
1	$\text{FASnI}_2(\text{SCN})$	12.630	13.070	12.694	89.97	90.00	90.00	Monoclinic
2	$\text{FASnI}(\text{SCN})_2$	12.673	12.676	12.647	89.93	89.96	89.97	Triclinic
3	$\text{FASn}(\text{SCN})_3$	14.088	13.884	13.736	83.87	83.36	91.19	Triclinic

**Table S2.** Bond lengths and angles of  $\text{FASnI}_{3-x}(\text{SCN})_x$  conventional cells, calculated using the PBE function.

Materials	Sn-X / $\text{\AA}$			$\angle \text{Sn-X-Sn} / \text{deg}$		
	Sn-I	Sn-S	Sn-N	$\angle \text{Sn-I-Sn}$	$\angle \text{Sn-N-Sn}$	$\angle \text{Sn-S-Sn}$
$\text{FASnI}_3$	3.16	-	-	180	-	-
$\text{FASnI}_2(\text{SCN})$	3.18-3.28	2.45	1.85	167.03	167.61	156.40
)						
$\text{FASnI}(\text{SCN})_2$	3.06-3.32	2.41-2.43	1.66-1.69	163.13	162.97	153.95
$\text{FASn}(\text{SCN})_3$	-	1.89-2.63	1.79-2.17	-	162.91	144.58

**Table S3.** Calculated enthalpy of formation ( $\Delta H_f$ ) for FASnI<sub>3-x</sub>(SCN)<sub>x</sub> tin perovskites.

Materials	$\Delta H_f$ /kcal mol <sup>-1</sup>
FASnI <sub>3</sub>	-34.6
FASnI <sub>2</sub> (SCN)	-51.6
FASnI(SCN) <sub>2</sub>	-50.2
FASn(SCN) <sub>3</sub>	-52.9

**Table S4.** Calculated Goldschmidt tolerance factor ‘ $\alpha$ ’ and octahedral factor ‘ $\mu$ ’ for FASnI<sub>3-x</sub>(SCN)<sub>x</sub> tin perovskites.

Materials	r <sub>A</sub>	r <sub>B</sub>	r <sub>X</sub> /pm		$\alpha$	$\mu$
Ionic species	FA <sup>+</sup>	Sn <sup>2+</sup>	I <sup>-</sup>	SCN <sup>-</sup>		
<b>FASnI<sub>3</sub></b>	253	103	215	-	1.04	0.48
<b>FASnI<sub>2</sub>(SCN)</b>	253	103	215	215	1.04	0.48
<b>FASnI(SCN)<sub>2</sub></b>	253	103	215	215	1.04	0.48
<b>FASn(SCN)<sub>3</sub></b>	253	103	-	215	1.04	0.48

**Table S5.** Comparison of stoichiometric ratios of Sn:S in  $\text{FASnI}_{3-x}(\text{SCN})_x$  perovskites.

Materials	Expected stoichiometric ratios (Sn:S)	Stoichiometric ratios from XPS (Sn:S)	Stoichiometric ratios from EDX (Sn:S)
<b>FASnI<sub>3</sub></b>	1:0	1:0	1:0
<b>FASnI<sub>2</sub>(SCN)</b>	1:1	1:1.07	1:1.42
<b>FASnI(SCN)<sub>2</sub></b>	1:2	1:1.90	1:2.17
<b>FASn(SCN)<sub>3</sub></b>	1:3	1:1.28	1:2.84

**Table S6.** Fitted lifetimes of PL decay profiles of perovskite samples with relative amplitudes shown in parentheses. The corresponding PL decay profiles are shown in Figure 2c.

Samples	$\tau_1$ (A <sub>1</sub> ) /ns	$\tau_2$ (A <sub>2</sub> ) /ns	$\tau_{\text{pl}}$ /ns
<b>FASnI<sub>3</sub></b>	0.54 (0.93)	1.7 (0.07)	<b>0.76</b>
<b>FASnI<sub>2</sub>(SCN)</b>	0.73 (0.85)	4.8 (0.15)	<b>2.92</b>
<b>FASnI(SCN)<sub>2</sub></b>	1.00 (0.78)	8.1 (0.22)	<b>5.94</b>

**Table S7.** Photovoltaic parameters of carbon-electrode perovskite solar cells fabricated for fresh cells with the best performance under simulated illumination (AM1.5G, power density 100 mW cm<sup>-2</sup>) as shown in Figure 3c.

Solar Cells	$J_{\text{sc}}$ /mA cm <sup>-2</sup>	$V_{\text{oc}}$ /V	FF	PCE /%
<b>FASnI<sub>3</sub></b>	16.60	0.177	0.311	0.9
<b>FASnI<sub>2</sub>(SCN)</b>	13.80	0.261	0.493	1.8
<b>FASnI(SCN)<sub>2</sub></b>	16.04	0.273	0.549	2.4
<b>FASn(SCN)<sub>3</sub></b>	0.25	0.028	0.221	0.001

**Table S8.** Photovoltaic parameters of the solution aged overnight shown in Figure S13.

Solar Cells	$J_{sc}$ /mA cm <sup>-2</sup>	$V_{oc}$ /V	FF	PCE /%
FASnI <sub>3</sub> (Overnight aged solution)	3.30	0.033	0.257	0.0
FASnI(SCN) <sub>2</sub> (Overnight aged solution)	14.61	0.264	0.496	1.9

**Table S9.** Photovoltaic parameters of carbon-electrode perovskite devices obtained from current–voltage curves shown in Figure 4a

Solar Cells		$J_{sc}$ /mA cm <sup>-2</sup>	$V_{oc}$ /V	FF	PCE /%
<b>PEA<sub>0.1</sub>FA<sub>0.9</sub>SnI(SCN)<sub>2</sub> (P10)</b>	best	17.46	0.326	0.493	2.8
	average	16.8±1.3	0.311±0.01	0.500±0.025	2.6±0.2
<b>PEA<sub>0.1</sub>FA<sub>0.9</sub>SnI(SCN)<sub>2</sub>+5% EDAI<sub>2</sub> (P10E5)</b>	best	20.17	0.322	0.574	3.7
	average	19.3±1.2	0.326±0.02	0.502±0.023	3.2±0.2

**Table S10.** Photovoltaic parameters of mesoscopic perovskite solar cells fabricated with FASnI<sub>3</sub> under illumination (AM-1.5G, power density 100 mW cm<sup>-2</sup>); active area 0.09 cm<sup>2</sup>.

Cell No.	$J_{sc}$ /mA cm <sup>-2</sup>	$V_{oc}$ /V	FF	PCE /%
<b>1</b>	18.9	0.142	0.315	<b>0.9</b>
<b>2</b>	12.7	0.157	0.410	<b>0.9</b>
<b>3</b>	19.7	0.148	0.293	<b>0.9</b>
<b>4</b>	15.2	0.159	0.354	<b>0.9</b>
<b>5</b>	19.8	0.146	0.294	<b>0.9</b>
<b>6</b>	17.3	0.154	0.320	<b>0.9</b>
<b>7</b>	19.3	0.146	0.294	<b>0.9</b>
<b>8</b>	16.7	0.152	0.326	<b>0.9</b>
<b>9</b>	18.7	0.147	0.325	<b>0.9</b>
<b>10</b>	17.5	0.148	0.310	<b>0.8</b>
<b>11</b>	18.8	0.139	0.297	<b>0.8</b>
<b>12</b>	17.0	0.145	0.295	<b>0.8</b>
<b>13</b>	18.4	0.133	0.290	<b>0.8</b>
<b>14</b>	14.8	0.144	0.331	<b>0.8</b>
<b>15</b>	16.1	0.142	0.339	<b>0.8</b>
<b>16</b>	21.2	0.129	0.282	<b>0.8</b>
<b>17</b>	13.0	0.137	0.348	<b>0.7</b>
<b>18</b>	14.9	0.132	0.335	<b>0.7</b>
<b>19</b>	18.7	0.130	0.287	<b>0.7</b>
<b>20</b>	13.9	0.141	0.334	<b>0.7</b>
<b>21</b>	17.7	0.126	0.294	<b>0.7</b>
<b>22</b>	14.3	0.140	0.343	<b>0.7</b>
<b>23</b>	19.8	0.117	0.278	<b>0.7</b>
<b>24</b>	14.3	0.141	0.335	<b>0.7</b>
<b>25</b>	17.3	0.124	0.285	<b>0.7</b>
<b>26</b>	14.7	0.143	0.334	<b>0.7</b>
<b>27</b>	12.2	0.128	0.346	<b>0.6</b>
<b>28</b>	12.5	0.126	0.333	<b>0.6</b>
<b>29</b>	13.1	0.133	0.347	<b>0.6</b>
<b>30</b>	16.6	0.177	0.311	<b>0.9</b>
<b>Average</b>	<b>17.0±2.1</b>	<b>0.138±0.01</b>	<b>0.309±0.023</b>	<b>0.8±0.1</b>

**Table S11.** Photovoltaic parameters of mesoscopic perovskite solar cells fabricated with FASnI(SCN)<sub>2</sub> under illumination (AM-1.5G, power density 100 mW cm<sup>-2</sup>); active area 0.09 cm<sup>2</sup>.

Cell No.	$J_{sc}$ /mA cm <sup>-2</sup>	$V_{oc}$ /V	FF	PCE/ %
<b>1</b>	16.0	0.275	0.549	<b>2.4</b>
<b>2</b>	16.0	0.276	0.540	<b>2.4</b>
<b>3</b>	16.0	0.270	0.450	<b>2.3</b>
<b>4</b>	18.8	0.270	0.460	<b>2.3</b>
<b>5</b>	18.3	0.272	0.473	<b>2.3</b>
<b>6</b>	17.4	0.260	0.506	<b>2.3</b>
<b>7</b>	17.0	0.292	0.480	<b>2.2</b>
<b>8</b>	16.0	0.277	0.470	<b>2.2</b>
<b>9</b>	17.2	0.262	0.474	<b>2.2</b>
<b>10</b>	16.6	0.279	0.510	<b>2.2</b>
<b>11</b>	15.9	0.281	0.470	<b>2.2</b>
<b>12</b>	17.9	0.276	0.503	<b>2.2</b>
<b>13</b>	15.5	0.276	0.486	<b>2.2</b>
<b>14</b>	16.2	0.273	0.500	<b>2.2</b>
<b>15</b>	16.0	0.281	0.476	<b>2.2</b>
<b>16</b>	16.2	0.271	0.490	<b>2.2</b>
<b>17</b>	16.1	0.258	0.460	<b>2.2</b>
<b>18</b>	16.3	0.281	0.506	<b>2.1</b>
<b>19</b>	16.6	0.283	0.5028	<b>2.1</b>
<b>20</b>	15.0	0.261	0.492	<b>2.1</b>
<b>21</b>	15.0	0.266	0.490	<b>2.1</b>
<b>22</b>	18.1	0.282	0.505	<b>2.1</b>
<b>23</b>	15.0	0.278	0.502	<b>2.1</b>
<b>24</b>	15.2	0.280	0.502	<b>2.1</b>
<b>25</b>	16.4	0.251	0.482	<b>2.1</b>
<b>26</b>	15.0	0.264	0.490	<b>2.1</b>
<b>27</b>	17.5	0.250	0.480	<b>2.1</b>
<b>28</b>	16.3	0.267	0.544	<b>2.1</b>
<b>29</b>	17.7	0.250	0.480	<b>2.1</b>
<b>30</b>	17.6	0.264	0.490	<b>2.1</b>
<b>Average</b>	<b>16.2±1.0</b>	<b>0.271±0.01</b>	<b>0.492±0.023</b>	<b>2.2±0.1</b>

**Table S12.** Photovoltaic parameters of mesoscopic perovskite solar cells fabricated with P10 under illumination (AM-1.5G, power density 100 mW cm<sup>-2</sup>); active area 0.09 cm<sup>2</sup>.

Cell No.	$J_{sc}$ /mA cm <sup>-2</sup>	$V_{oc}$ /V	FF	PCE /%
<b>1</b>	17.1	0.305	0.485	<b>2.6</b>
<b>2</b>	16.9	0.285	0.481	<b>2.4</b>
<b>3</b>	19.2	0.307	0.467	<b>2.8</b>
<b>4</b>	17.8	0.307	0.478	<b>2.6</b>
<b>5</b>	16.7	0.323	0.484	<b>2.6</b>
<b>6</b>	17.5	0.326	0.494	<b>2.9</b>
<b>7</b>	17.6	0.326	0.489	<b>2.8</b>
<b>8</b>	17.1	0.324	0.498	<b>2.8</b>
<b>9</b>	17.2	0.322	0.499	<b>2.8</b>
<b>10</b>	14.9	0.330	0.514	<b>2.6</b>
<b>11</b>	15.5	0.330	0.514	<b>2.7</b>
<b>12</b>	15.2	0.330	0.524	<b>2.7</b>
<b>13</b>	15.6	0.320	0.515	<b>2.6</b>
<b>14</b>	15.7	0.320	0.520	<b>2.7</b>
<b>15</b>	17.2	0.312	0.496	<b>2.7</b>
<b>16</b>	15.5	0.300	0.514	<b>2.4</b>
<b>17</b>	14.5	0.300	0.534	<b>2.4</b>
<b>18</b>	14.8	0.299	0.518	<b>2.3</b>
<b>19</b>	15.9	0.292	0.519	<b>2.4</b>
<b>20</b>	16.4	0.289	0.514	<b>2.5</b>
<b>21</b>	14.8	0.292	0.578	<b>2.5</b>
<b>22</b>	17.4	0.307	0.499	<b>2.7</b>
<b>23</b>	18.1	0.293	0.492	<b>2.7</b>
<b>24</b>	16.5	0.303	0.510	<b>2.6</b>
<b>25</b>	17.1	0.305	0.485	<b>2.6</b>
<b>26</b>	19.2	0.307	0.467	<b>2.8</b>
<b>27</b>	17.8	0.307	0.478	<b>2.6</b>
<b>28</b>	18.6	0.322	0.452	<b>2.8</b>
<b>29</b>	17.4	0.32	0.484	<b>2.7</b>
<b>30</b>	17.9	0.306	0.504	<b>2.8</b>
<b>Average</b>	<b>16.8±1.3</b>	<b>0.311±0.01</b>	<b>0.500±0.025</b>	<b>2.6±0.2</b>

**Table S13.** Photovoltaic parameters of mesoscopic perovskite solar cells fabricated with P10E5 under illumination (AM 1.5G, power density 100 mW cm<sup>-2</sup>); active area 0.09 cm<sup>2</sup>.

Cell No.	$J_{sc}$ mA cm <sup>-2</sup>	$V_{oc}$ /V	FF	PCE /%
<b>1</b>	19.6	0.324	0.521	<b>3.3</b>
<b>2</b>	20.0	0.301	0.514	<b>3.1</b>
<b>3</b>	19.2	0.361	0.469	<b>3.3</b>
<b>4</b>	18.0	0.35	0.477	<b>3.0</b>
<b>5</b>	17.4	0.342	0.516	<b>3.1</b>
<b>6</b>	19.9	0.301	0.507	<b>3.1</b>
<b>7</b>	17.5	0.34	0.508	<b>3.1</b>
<b>8</b>	17.6	0.339	0.511	<b>3.1</b>
<b>9</b>	21.2	0.304	0.499	<b>3.2</b>
<b>10</b>	17.8	0.337	0.503	<b>3.1</b>
<b>11</b>	17.9	0.336	0.504	<b>3.1</b>
<b>12</b>	18.2	0.333	0.497	<b>3.0</b>
<b>13</b>	18.9	0.33	0.482	<b>3.0</b>
<b>14</b>	19.7	0.323	0.496	<b>3.2</b>
<b>15</b>	19.1	0.316	0.511	<b>3.1</b>
<b>16</b>	19.9	0.327	0.537	<b>3.5</b>
<b>17</b>	20.2	0.322	0.574	<b>3.7</b>
<b>18</b>	19.0	0.341	0.463	<b>3.0</b>
<b>19</b>	19.2	0.324	0.51	<b>3.2</b>
<b>20</b>	19.2	0.326	0.508	<b>3.2</b>
<b>21</b>	22.4	0.329	0.465	<b>3.5</b>
<b>22</b>	21.2	0.326	0.473	<b>3.3</b>
<b>23</b>	19.3	0.326	0.505	<b>3.2</b>
<b>24</b>	20.2	0.332	0.501	<b>3.4</b>
<b>25</b>	19.2	0.332	0.509	<b>3.3</b>
<b>26</b>	18.7	0.307	0.496	<b>2.9</b>
<b>27</b>	19.7	0.301	0.501	<b>3.0</b>
<b>28</b>	20.5	0.297	0.507	<b>3.1</b>
<b>29</b>	17.5	0.34	0.517	<b>3.1</b>
<b>30</b>	17.7	0.338	0.509	<b>3.1</b>
<b>Average</b>	<b>19.3±1.2</b>	<b>0.326±0.02</b>	<b>0.502±0.023</b>	<b>3.2±0.2</b>

**Table S14.** Fitted EIS parameters of the devices; the corresponding Nyquist plots are shown in Figure S24.

Solar Cells	R <sub>0</sub>	R <sub>ct</sub>	C <sub>ct</sub> -T	C <sub>ct</sub> -P	R <sub>rec</sub>	C <sub>rec</sub> -T	C <sub>rec</sub> -P
<b>FASnI<sub>3</sub></b>	24.32	7.73	$2.06 \times 10^{-5}$	0.751	111.8	$14.0 \times 10^{-5}$	0.848
<b>FASnI(SCN)<sub>2</sub></b>	28.94	13.90	$1.86 \times 10^{-7}$	0.990	313.4	$2.19 \times 10^{-6}$	0.972
<b>P10</b>	28.46	11.54	$5.56 \times 10^{-7}$	0.911	356.3	$3.02 \times 10^{-6}$	0.874
<b>P10E5</b>	23.45	7.27	$5.34 \times 10^{-7}$	0.965	566.1	$1.99 \times 10^{-6}$	0.938

**Table S15.** Photovoltaic parameters of fresh devices and devices after storage for 6 h under ambient conditions without encapsulation as the *J-V* curves shown in Figure S26b

Solar Cells	J <sub>sc</sub> /mA cm <sup>-2</sup>	V <sub>oc</sub> /V	FF	PCE /%
FASnI <sub>3</sub> (fresh)	14.35	0.155	0.311	0.7
FASnI <sub>3</sub> (after 6 h)	0.94	0.004	NAN	0.0
FASnI(SCN) <sub>2</sub> (fresh)	15.04	0.269	0.490	2.0
FASnI(SCN) <sub>2</sub> (after 6 h)	16.48	0.234	0.421	1.6
P10 (fresh)	18.08	0.302	0.491	2.7
P10 (after 6 h)	19.40	0.265	0.453	2.3
P10E5 (fresh)	19.86	0.327	0.533	3.5
P10E5 (after 6 h)	19.51	0.324	0.520	3.3

## References

- (S1) Filby, A. G.; Howie, R. A.; Moser, W. The Structure of Tin(II) Thiocyanate. *J. Chem. Soc. Dalt. Trans.* **1978**, 12, 1797–1799.
- (S2) Grimme, S. Semiempirical GGA-type Density Functional Constructed with a Long-Range Dispersion Correction. *J. Comput. Chem.* **2006**, 27, 1787–1799.
- (S3) Perdew, J. P.; Burke, K.; Ernzerhof, M. Generalized Gradient Approximation Made Simple. *Phys. Rev. Lett.* **1996**, 77, 3865–3868.
- (S4) Jenkins, H. D. B.; Thakur, K. P. Reappraisal of Thermochemical Radii for Complex Ions. *J. Chem. Educ.* **1979**, 56, 576–577.
- (S5) Stoumpos, C. C.; Malliakas, C. D.; Kanatzidis, M. G. Semiconducting Tin and Lead Iodide Perovskites with Organic Cations: Phase Transitions, High Mobilities, and Near-Infrared Photoluminescent Properties. *Inorg. Chem.* **2013**, 52, 9019–9038.